ACS APPLIED MATERIALS & INTERFACES

Research Article

www.acsami.org

Layer-Dependent Dopant Stability and Magnetic Exchange Coupling of Iron-Doped MoS_2 Nanosheets

Haibo Shu,*[,†,‡] Pengfei Luo,[†] Pei Liang,[†] Dan Cao,[§] and Xiaoshuang Chen[‡]

[†]College of Optical and Electronic Technology and [§]College of Science, China Jiliang University, 310018 Hangzhou, China

[‡]National Laboratory for Infrared Physics, Shanghai Institute of Technical Physics, Chinese Academy of Science, 200083 Shanghai, China

Supporting Information

ABSTRACT: Using density-functional theory calculations including a Hubbard *U* term we explore structural stability, electronic and magnetic properties of Fe-doped MoS_2 nanosheets. Unlike previous reports, the geometry and the stability of Fe dopant atoms in MoS_2 nanosheets strongly depend on the chemical potential and the layer number of sheets. The substitution Fe dopant atoms at the Mo sites are energetically favorable in monolayer MoS_2 and the formation of intercalated and substitutional Fe complexes are preferred in bilayer and multilayer ones under the S-rich regime that is a popular condition for the synthesis of MoS_2 nanosheets. We find that the Fe dopants prefer to the ferromagnetic coupling in monolayer MoS_2 and the antiferromagnetic coupling in bilayer and multilayer ones, suggesting the layer dependence of magnetic exchange coupling (MEC). The transition of MEC in Fe-doped MoS_2 sheets induced by the change of layer number arises from the competition mechanism between the double-exchange and superexchange couplings. The findings provide a route to facilitate the design of MoS_2-based diluted magnetic semiconductors and spintronic devices.

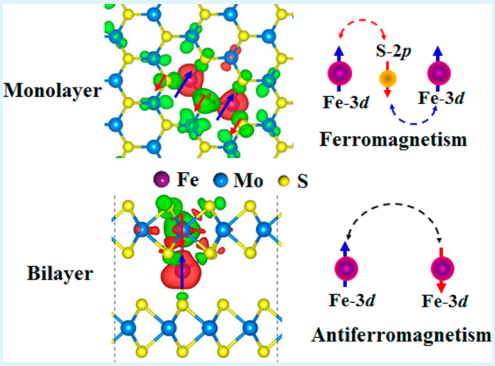

KEYWORDS: *molybdenum disulfide, nanosheet, dopant stability, magnetic exchange coupling, density functional theory*

1. INTRODUCTION

Two dimensional (2D) nanomaterials such as graphene, silicene, hexagonal BN, and transition metal dichalcogenides (TMDs),[1−6] have received great interest in the past decade because of their unique physical properties and technological importance in developing the future nanoscale devices. Among these 2D nanomaterials, atomic-layered MoS_2 is one of the most extensively studied targets because they exhibit many outstanding physical and chemical properties, including of medium intrinsic band gap (1.3−1.8 eV),[7] ultrafast saturable absorption,[8] higher catalytic activity,[9] and novel valley polarization properties,[10] which make them an important candidate material for the applications in nanoscale field-effect transistors,[11] phototransistors,[12] sensors,[13] lithium-ion battery,[14,15] and photocatalysts.[16] On the basis of the concept of diluted magnetic semiconductor (DMS), manipulating the magnetic properties of MoS_2 nanosheets is crucial for expanding their applications in nanoelectronics and spintronics. However, pristine MoS_2 nanosheets are intrinsically nonmagnetic. Therefore, the realization of stable magnetism in MoS_2 is highly desirable.

Motivated by the potential applications and the great demands for magnetic MoS_2 nanostructures, a variety of methods have been developed and explored in past few years. Largely, the magnetism of 2D materials can be realized by the following ways: (i) the introduction of defects,[17,18] (ii) surface functionalization (i.e., hydrogenation),[19] (iii) cutting 2D nanosheets into one-dimensional (1D) nanoribbons (NRs),[20,21] and (iv) the transition-metal (TM) doping.[22,23] As far as MoS_2 is concerned, the magnetism induced by methods (i) strongly depends on the defect configurations. Moreover, large system magnetism requires the introduction of a large number of defects into MoS_2 sheet,[17,18] which may result in the reduction of carrier mobility because of the formation of scattering centers or charge-trapping sites in the MoS_2 sheets. Although method (ii) can produce stable magnetism, the surface hydrogenation of MoS_2 realized in experiment presents a big challenge. For instance, the surface hydrogenation requires the implementation of an external stress in MoS_2 nanosheets.[19] For method (iii), the magnetism of MoS_2 NRs depends on their edge types. The zigzag NRs exhibit ferromagnetic behavior but the armchair NRs are nonmagnetic.[20] This implies that the edge of MoS_2 NRs needs to be well-controlled.[21] In contrast, for method (iv), the TM doping is a facile and conventional way to obtain stable magnetism in 2D semiconductor materials. Moreover, the magnitude of magnetism and the dopant concentration of MoS_2 nanosheets can be controlled in the doping process.

To obtain the stable magnetism of 2D MoS_2 nanomaterials, a large number of theoretical studies have been devoted to the

Received: December 15, 2014
Accepted: March 24, 2015
Published: March 24, 2015

DOI: 10.1021/am508843z
ACS Appl. Mater. Interfaces 2015, 7, 7534−7541

exploration of TM-doped MoS_2 nanosheets.[24−30] Cheng et al.[24] reported theoretically the realization of 2D-DMS in monolayer MoS_2 by the introduction of Mn, Fe, Co, Zn, and Hg dopants. The Mn dopant was demonstrated as an effective dopant to induce the ferromagnetism of MoS_2 monolayer.[26] Moreover, the predicted Curie temperature of Mn-doped MoS_2 can reach room temperature when the doping concentration of Mn increases in the range of 10−15%.[27] On the other hand, the magnetism of MoS_2 monolayer was also achieved by substituting nonmetal elements (e.g., F and Cl) into the S sites,[31] but the dopants in MoS_2 display higher formation energies and thus have lower dopant concentration. The recent theoretical studies carried out by Feng et al.[32] reported that the cluster doping could be a feasible strategy for the realization of ferromagnetism in monolayer MoS_2 by introducing Fe-X (X = S, C, N, O, and F) clusters. Apart from the studies of magnetic doping in monolayer MoS_2, the doping in bilayer MoS_2 sheets has also been carried out in recent years. On the basis of density-functional calculations, bilayer MoS_2 was found to exhibit high spin-polarization by the intercalation of magnetic dopants (e.g., Fe and Mn) into the bilayer sheet.[33,34] The previous theoretical studies provide a solid foundation to insight into magnetic properties of doped 2D-MoS_2 nanomaterials, but most of results presented in these literatures were obtained on the basis of presupposed models in which the doping sites are set at either the substitution sites (Mo or S atoms) of monolayer MoS_2 or the interlayer interstitial sites of bilayer one. It is a well-known fact that the doping sites and the dopant distribution in the host materials depend on the synthesis conditions. Adjusting the growth conditions, including S/Mo ratio or temperature, may result in the change of doping configurations. More importantly, the magnetic exchange interaction among dopants in the host material is sensitive to the growth conditions. Hence, it is necessary to understand the dopant stability and magnetic coupling mechanism of doped 2D-MoS_2 under different growth environments.

In this work, we perform a comprehensive theoretical investigation of thermodynamic stability, spin-polarized electronic and magnetic properties of Fe-doped MoS_2 nanosheets by using density-functional (DFT) calculations. Our results demonstrate that the doping configuration and the magnetic exchange coupling (MEC) of Fe-doped MoS_2 nanosheets are dependent on the chemical potential and the layer number. We find that the ferromagnetism of MoS_2 is easily realized in the monolayer structure and the antiferromagnetic (AFM) coupling is more favorable for bilayer and multilayer ones in most of chemical potential conditions. The present results suggest the importance of the control of layer number of sheets and growth conditions in the design of MoS_2-based DMS.

2. COMPUTATIONAL DETAILS

The doping structures of Fe-doped MoS_2 nanosheets are created on the basis of a (4 × 4) supercell. The use of this model ensures that the distance among dopants with the adjacent images is larger than 12 Å. This is sufficient to avoid interactions between Fe dopants in neighboring unit cells. The MoS_2 nanosheets with in-plane periodicity are separated by ∼15 Å vacuum layers to prohibit the interactions of neighboring images. The thermodynamic stability of Fe dopant atoms in MoS_2 nanosheets is evaluated by calculating their formation energies (E_f) as follows

$$E_f = E_T - E_P - \Delta n_{Mo}\mu_{Mo} - \Delta n_S\mu_S - \Delta n_{Fe}\mu_{Fe} \quad (1)$$

where E_T and E_P are the energies of Fe-doped and perfect MoS_2 sheets respectively, μ_i is the chemical potential of the atomic species i (i = Mo, S, and Fe), and Δn_i is the difference of atomic species i in the Fe-doped and perfect MoS_2 nanosheets. To maintain a thermodynamic equilibrium of crystalline phase ($\mu_{Mo} + 2\ \mu_S = \mu_{MoS2}$), the allowable value of μ_S is $\mu_{S(bulk)}$-$\Delta H_f < \mu_S < \mu_{S(bulk)}$, where the upper (lower) limit corresponds to S-rich (Mo-rich) condition and ΔH_f is the heat of formation of MoS_2 nanosheets. The computed heat of formation is 1.24 eV, which is in good agreement with previous theoretical report.[35] Using a few algebraic steps, eq 1 can be expressed as

$$E_f = E_T - E_P - \Delta n_{Mo}\mu_{MoS2} - (\Delta n_S - \Delta n_{Mo})\mu_S - \Delta n_{Fe}\mu_{Fe} \quad (2)$$

All calculations in the present work are performed by using the DFT as implemented in the Vienna ab initio Simulation Package (VASP).[36,37] To treat accurately the exchange and correlation of Fe-3d states, we use spin-polarized generalized-gradient approximation (GGA) of Perdew−Burke−Ernzerhof.[38] However, the GGA functional fails to describe partially occupied d and f electronic states of transition metal elements.[39] Therefore, the GGA with the correction of a Hubbard U term is used in the present study. For the Hubbard parameter $U_{eff} = U - J$, we use a typical value of 4 eV that was proved a reasonable value to describe the correlation energy of localized Fe-3d states on the basis of the careful tests of electronic structures and magnetic interactions, and the details are shown in S1 of Supporting Information. Moreover, the U_{eff} = 4 eV was widely adopted in previous investigations of Fe-doped systems.[40−42] The electron−ion interactions were described by projector augmented wave (PAW) potentials.[43] The kinetic energy cutoff for the plane-wave expansion is set to 400 eV and it is found that the cutoff energy can provide sufficient accuracy based on the tests of energy and magnetism. For the geometry optimization, the convergence criteria of electronic and ionic iterations are 1×10^{-3} eV and 1×10^{-2} eV/Å. The Bader charge analysis[44,45] was carried out to examine the charge transfers among Fe dopants, Mo, and S atoms in these doped MoS_2 sheets.

3. RESULTS

3.1. Isolated Fe Dopant in Monolayer MoS_2. First, we have studied the geometry, structure, and magnetic properties of isolated Fe dopant atom in monolayer MoS_2 with the purpose of elucidating which doping configurations are the most stable. We have considered five doping configurations (Figure 1a): substitutional Fe at the Mo site (Fe_{Mo}),

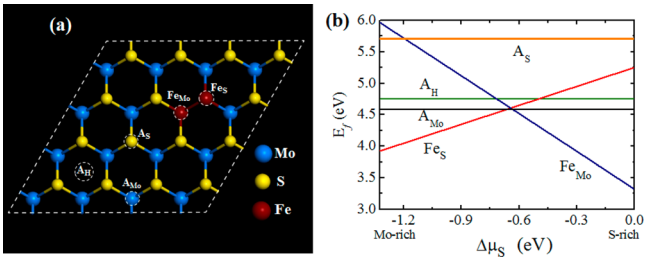

Figure 1. (a) Doping configurations (top view) and (b) formation energies of isolated Fe dopant atom at different doping sites of monolayer MoS_2. The potential doping sites include two substitution sites (Fe_{Mo} and Fe_S) and three adsorption sites (A_S, A_{Mo}, and A_H). Mo, S, and Fe atoms are colored by blue, yellow, and red balls, respectively.

substitutional Fe at the S site (Fe_s), and Fe adatoms (A_{Mo}, A_S, and A_H). A_{Mo}, A_S, and A_H are the Fe adatom on the top of Mo atom, the top of S atom, and at the hollow site, respectively. The formation energies of five doping structures as a function of S chemical potential difference ($\Delta\mu_S = \mu_S - \mu_{S(bulk)}$) have been shown in Figure 1b. It is found that Fe_S is the most stable doping configuration in the Mo-rich condition ($\Delta\mu_S < -0.67$

DOI: 10.1021/am508843z
ACS Appl. Mater. Interfaces 2015, 7, 7534−7541

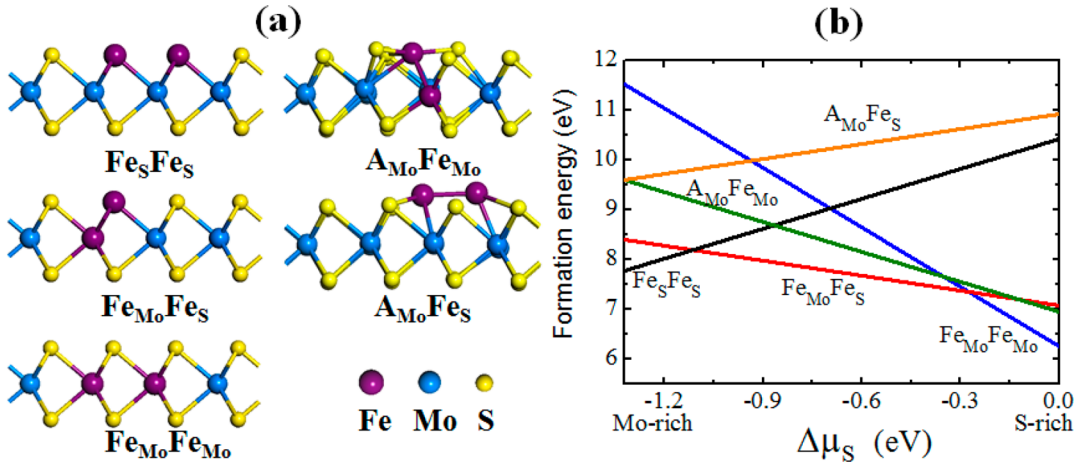

Figure 2. (a) Optimized doping atomic configurations (side view) and (b) formation energies of two Fe impurities in monolayer MoS_2. Five potential doping configurations are $Fe_{Mo}Fe_{Mo}$, $Fe_{Mo}Fe_S$, and Fe_SFe_S, respectively. Mo, S, and Fe atoms are colored by blue, yellow, and purple balls, respectively.

eV) and Fe_{Mo} is energetically favorable under the S-rich regime ($\Delta\mu_S > -0.63$ eV). For the three Fe adatoms, only A_{Mo} is stable at a medium chemical potential condition (e.g., $\Delta\mu_S = -0.65$ eV), but the stable region of chemical potential is very small (~0.04 eV) and thus it is difficult to control in an experiment. The result suggests that Fe dopant atoms prefer to occupy the substitutional lattice sites of monolayer MoS_2, which agrees with the experimental observations that the cation doping in MoS_2 behaves as a substitution defect.[46]

The Fe_{Mo}, Fe_S, and A_{Mo} dopants in a (4 × 4) supercell produce overall magnetic moments (MMs) of 2.05 μ_B, 3.76 μ_B, and 3.29 μ_B, respectively. The overall MMs mainly correspond to the spin polarization (SP) of excess d electrons provided by the Fe dopant. The difference of MM of three doping configurations originates from the different doping environments. For the Fe_{Mo} structure, one part of valence electrons ($3d^64s^2$) of Fe dopant transfer to the nearest-neighboring S atoms and the two remnant valence electrons results in the system magnetism due to the spin polarization. The result is in good agreement with the previous prediction for the Fe_{Mo} magnetism with the MM of 1.93−2.0 μ_B.[24,25,29,32] In contrast, the nearest neighbors of Fe dopant in the Fe_S structure are Mo atoms and there are relatively fewer charge transfers between Fe and Mo atoms, resulting in localized electrons around the Fe and Mo atoms. The calculated Bader charges of Fe and Mo atoms in the Fe_S structure are 0.27 e and 0.21 e larger than those in the Fe_{Mo} structure, respectively. Therefore, the Fe_S structure has the larger MM than the Fe_{Mo} structure when the localized electrons are polarized. Such a result can be confirmed by the spin-density ($\rho\uparrow - \rho\downarrow$) distributions (Figure S3 in the Supporting Information). It can be found that the spin-polarized electrons locate around not only Fe atom but also the neighboring Mo atom in the Fe_S structure. For the A_{Mo} structure, the charge transfer from Fe adatom to MoS_2 sheet is small because of the chemical stability of MoS_2 monolayer, and thus the system magnetism of A_{Mo} is almost from the SP of Fe atom (Figure S3 in the Supporting Information).

3.2. Magnetic Exchange Coupling of Fe-Doped Monolayer MoS_2. To investigate the MEC of Fe-doped MoS_2 monolayer, we introduced two Fe dopants into the host material. On the basis of the stability of isolate Fe dopant in monolayer MoS_2, introducing two Fe dopant atoms can create five different doping configurations. As shown in Figure 2a, they are Fe_SFe_S, $Fe_{Mo}Fe_S$, $Fe_{Mo}Fe_{Mo}$, $A_{Mo}Fe_{Mo}$, and $A_{Mo}Fe_S$, respectively. Figure 2b shows the formation energies of five doping structures as a function of S chemical potential. We find that Fe_SFe_S is stable under Mo-rich conditions, $Fe_{Mo}Fe_{Mo}$ becomes the most stable configuration in the S-rich regime ($\Delta\mu_S > -0.56$ eV), and $Fe_{Mo}Fe_S$ is stable when $\Delta\mu_S$ lies between −1.27 and −0.56 eV. For $A_{Mo}Fe_{Mo}$ and $A_{Mo}Fe_S$, they are still energetically unfavorable in the allowed range of S chemical potential (Figure 2b). In other words, Fe dopants prefer to occupy at substitutional sites in MoS_2 monolayer. Previous experimental studies have found that the synthesis of MoS_2 nanosheets requires a chemical environment of high S/Mo ratio (S/Mo > 2)[47,48] so as to ensure the crystallization of MoS_2. This implies that $Fe_{Mo}Fe_{Mo}$ is more easily achieved than other doping structures. It needs to be noted that there is the possibility of causing the structural phase transition of MoS_2 from the 2H phase to 1T phase through the adsorption and doping of metallic ions.[49,50] To investigate the possibility of phase transition, we make an energy comparison between Fe-doped MoS_2 monolayer with 1T and 2H phases. Using a (4 × 4) supercell, the calculated results indicate that the total energies of Fe_{Mo}, Fe_S, and A_H in 2H phase (see Figure 1) are 8.76, 8.34, and 8.89 eV lower than that of their 1T phase, correspondingly. Increasing the dopant concentration from one Fe dopant to two dopants, we find that Fe-doped MoS_2 systems in 2H phase are still more stable than their 1T phase. For example, the energy of $Fe_{Mo}Fe_{Mo}$ in 2H phase is 6.40 eV lower than that of their 1T phase. Therefore, there is impossible to induce the structural phase transition of Fe-doped MoS_2 in a dilute magnetic regime with the dopant concentration of <12.5%.

The magnetic exchange coupling of Fe-doped MoS_2 monolayer is first evaluated by the energy comparison of ferromagnetic (FM) and antiferromagnetic (AFM) states as follows

$$\Delta E = E_{AFM} - E_{FM} \quad (3)$$

where E_{AFM} and E_{FM} are the energies of Fe-doped MoS_2 in their AFM and FM states, respectively. The calculated result indicates that all three doping configurations have the FM ground state and the energies of Fe_SFe_S, $Fe_{Mo}Fe_S$, and $Fe_{Mo}Fe_{Mo}$ in their FM state are 20, 247, and 202 meV lower than that of their AFM state, respectively. Generally, a large ΔE

DOI: 10.1021/am508843z
ACS Appl. Mater. Interfaces 2015, 7, 7534−7541

is in favor of high-temperature FM system based on the mean-field theory and Heisenberg model.[51,52] Thus, implementing the Fe doping at the S-rich regime will contribute to the doped MoS_2 sheet with a high-temperature ferromagnetism. The FM coupling interactions of Fe-doped monolayer MoS_2 are further examined by the spin density distribution, as shown in Figure 3.

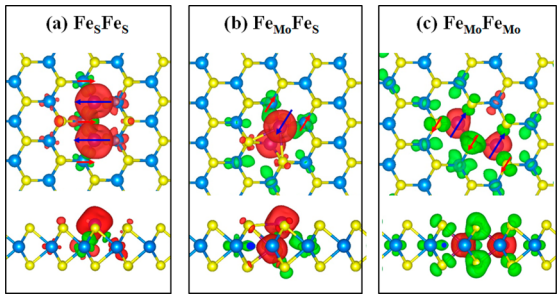

Figure 3. Top and side view of spin-density ($\rho\uparrow - \rho\downarrow$) isosurfaces of three Fe-doped monolayer MoS_2 systems: (a) Fe_SFe_S, (b) $Fe_{Mo}Fe_S$, and (c) $Fe_{Mo}Fe_{Mo}$. The red and green isosurfaces represent positive and negative spin density, respectively. The blue and red arrows denote the opposite direction of spin polarization.

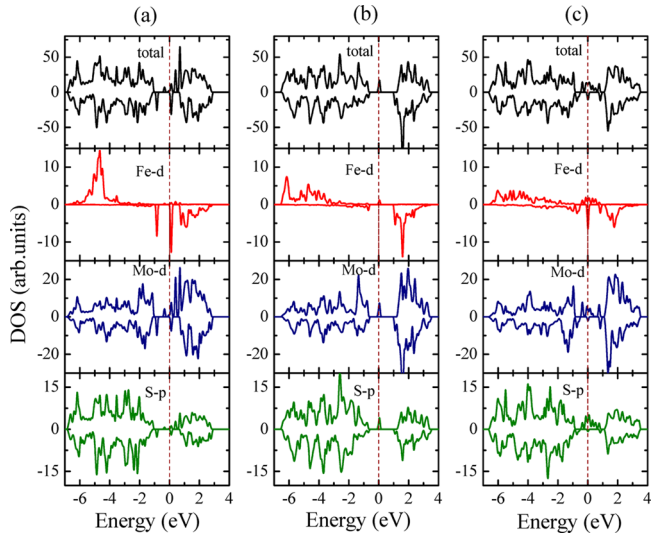

Figure 4. Total and partial density of states of Fe-doped monolayer MoS_2 in three doping configurations: (a) Fe_SFe_S, (b) $Fe_{Mo}Fe_S$, and (c) $Fe_{Mo}Fe_{Mo}$. The Fermi level is set to energy zero.

In all three doping configurations, Fe dopant atoms are highly spin-polarized and have the same spin-polarization direction, and the nearest neighboring (NN) Mo atoms between two Fe dopants are antiferromagnetically coupled with the Fe atoms. The magnetic interactions between Fe atoms in MoS_2, as obtained from our calculations, is very similar to the previous reports,[26,53] where the authors claimed the AFM coupling between TM spins and neighboring S spins and the FM coupling among TM spins that is governed by double exchange interactions.[54] Although all three doping systems exhibit the FM characteristic, they have different system magnetic moments. The calculated MMs are 6.56 μ_B, 5.98 μ_B, and 3.78 μ_B for Fe_SFe_S, $Fe_{Mo}Fe_S$, and $Fe_{Mo}Fe_{Mo}$, respectively. The difference in magnetism in the three structures mainly arises from different MMs between the Fe_{Mo} and the Fe_S dopants.

To gain further insight into the magnetic coupling interactions of Fe-doped monolayer MoS_2, we investigated the electronic density of states and band structures, as shown in Figure 4 and Figure S4 in the Supporting Information. It can be found that the introduction of Fe dopants in all three doping configurations leads to the impurity states at the vicinity of Fermi level. For the Fe_SFe_S structure (Figure 4a and Figure S4a in the Supporting Information), the Fe doping in MoS_2 monolayer produces two localized donor-like electronic states that locate at 0.29 eV above the valence band (VB) and 0.58 eV below the conduction band (CB), respectively. It can be found that the Fe-3d states are nearly spin-polarized and become the main contribution of system magnetism. The high-energy Mo-4d states (above −2 eV) indicate partial SP but the low-energy electronic states (below −2 eV) are nearly degenerate, whereas the S-3p states are nearly degenerate and mainly locate in the energy range from −6 to −1 eV. Therefore, there is a strong hybridization between the Mo-4d states and the S-3p states. For the $Fe_{Mo}Fe_{Mo}$ structure (Figure 4c and Figure S4c in the Supporting Information), it also shows a typical n-type doping characteristic. We find that the Fe-3d states are delocalized as compared to that of Fe_SFe_S and hybridized with S-3p states, resulting in the formation of Fe−S bonds. The polarized Fe-3d electrons in the $Fe_{Mo}Fe_{Mo}$ system are obviously weaker than that of Fe_SFe_S. It can be found that the p−d hybridization causes that spin-up S-2p states are shifted to higher energies and spin-down S-2p states are shifted to lower energies (see Figure 4c), leading to a local MM that is antiparallel to that of Fe atoms. Meanwhile, the SP direction of d electrons of the NN Mo atoms is antiparallel to that of Fe dopant, which is responsible for the relatively small overall MM of $Fe_{Mo}Fe_{Mo}$. For the $Fe_{Mo}Fe_S$, the Fe doping induces a deep impurity level that mainly arises from Mo-4d and S-3p states (see Figure 4b and Figure S4b in the Supporting Information). Similar to the case of $Fe_{Mo}Fe_{Mo}$, the SP of Fe-3d states and the partial SP of Mo-4d states is responsible for the system magnetism of $Fe_{Mo}Fe_S$.

3.3. Fe-Doped Bilayer MoS_2. We now turn to investigate structural and magnetic properties of Fe-doped bilayer MoS_2. Seven potential doping configurations have been considered here (see Figure 5a): (i) two Fe_{Mo} dopants in the same layer [denoted by $Fe_{Mo}Fe_{Mo}(S)$], (ii) two Fe_{Mo} dopants in different layers [denoted by $Fe_{Mo}Fe_{Mo}(D)$], (iii) Fe_{Mo} and Fe_S dopants in different layer (denoted by $Fe_{Mo}Fe_S$), (iv) two Fe_S dopants in different layers (denoted by Fe_SFe_S), (v) an intercalated Fe atom (Fe_i) and a Fe_{Mo} dopant (denoted by $Fe_{Mo}Fe_i$), (vi) Fe_i and Fe_S complex (denoted by Fe_SFe_i), and (vii) Fe_i and Fe_i complex (denoted by Fe_iFe_i). The formation energies of seven doping configurations as a function of S chemical potential have been shown in Figure 5b. It can be found that Fe_SFe_i is stable under the Mo-rich condition and Fe_iFe_i becomes the most stable doping structure when the S chemical potential $\Delta\mu_S$ is located in the range from −1.09 to −1.04 eV. When the S chemical potential difference $\Delta\mu_S$ is beyond −1.04 eV, $Fe_{Mo}Fe_i$ is energetically favorable. The three stable doping configurations appeared in different chemical potential regions have a common structural characteristic: there is a direct chemical bonding between two Fe dopants. The formation of Fe−Fe bonds in these structures enhances the layer interactions and contributes to the reduction of system energy. In contrast, the Fe doping in different layer of bilayer MoS_2 presents similar electronegativity, leading to the interlayer Coulomb repulsion. Therefore, the doping configurations of $Fe_{Mo}Fe_{Mo}(D)$, $Fe_{Mo}Fe_S$, and Fe_SFe_S are still metastable state (Figure 5b). The result is

DOI: 10.1021/am508843z
ACS Appl. Mater. Interfaces 2015, 7, 7534−7541

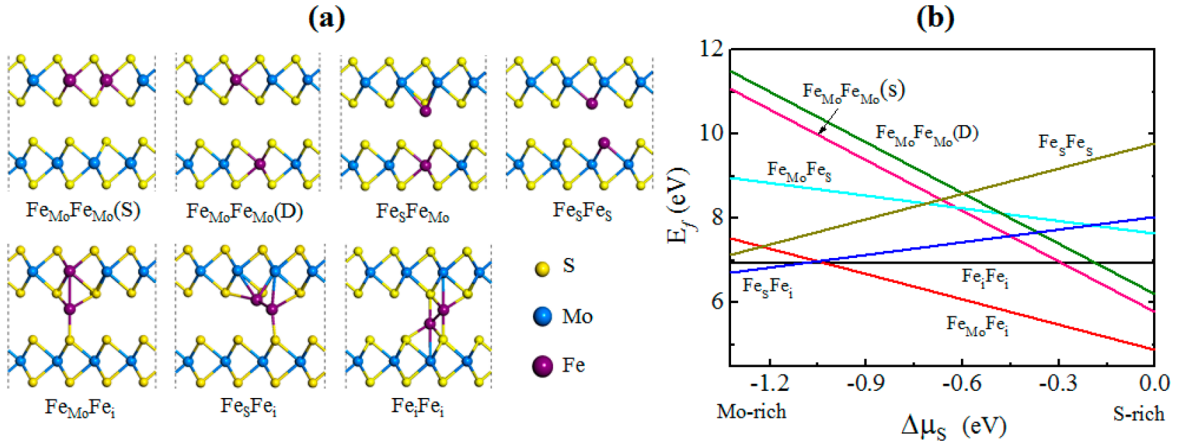

Figure 5. (a) Doping atomic configurations and (b) formation energies of Fe-doped bilayer MoS_2. Mo, S, and Fe atoms are colored by blue, yellow, and purple balls, respectively.

different from the case of Fe doping in monolayer MoS_2, suggesting that the intercalated Fe atom plays an important role in stabilizing doped bilayer MoS_2 system.

The magnetic ground state of three stable doping configurations listed above is evaluated by $\Delta E = E_{AFM} - E_{FM}$. The calculated ΔE is −6, 234, and −7 meV for Fe_SFe_i, Fe_iFe_i, and $Fe_{Mo}Fe_i$ systems, respectively. The result means that Fe_SFe_i and $Fe_{Mo}Fe_i$ have an AFM ground state and the ground state of Fe_iFe_i is ferromagnetic. Because of the very small stable region of chemical potential for the Fe_iFe_i system, the Fe-doped MoS_2 bilayer with the AFM coupling is more possible achieved in experiment. Such a result is different from the Fe-doped monolayer with the FM coupling. Figure 6 shows spin-density

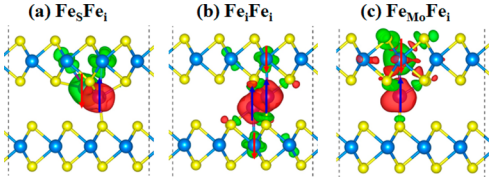

Figure 6. Spin-density ($\rho\uparrow - \rho\downarrow$) isosurface distributions of three Fe-doped bilayer MoS_2 systems: (a) Fe_SFe_i, (b) Fe_iFe_i, and (c) $Fe_{Mo}Fe_i$. The red and green isosurfaces represent positive and negative spin density, respectively. The blue and red arrows denote the opposite direction of spin polarization.

spatial distributions of Fe_SFe_i, Fe_iFe_i, and $Fe_{Mo}Fe_i$. For Fe_SFe_i and $Fe_{Mo}Fe_i$ structures (see Figure 6a, c), it is found that the interaction of two Fe dopants followed the superexchange coupling[54] has the opposite SP, leading to the AFM coupling. Because the AFM coupling between Fe dopants, Fe_SFe_i and $Fe_{Mo}Fe_i$ structures have the relatively smaller system magnetism. The calculated MMs of Fe_SFe_i and $Fe_{Mo}Fe_i$ are 1.33 μ_B and 0.14 μ_B, respectively. In contrast, the double-exchange coupling dominates the interaction of Fe dopants in Fe_iFe_i structure that is mediated by the NN S atoms (see Figure 6b) and thus the doping configuration has a larger overall MM (4.76 μ_B). Meanwhile, the Fe dopants negatively polarize their NN Mo atoms of MoS_2 bilayer, leading to an AFM coupling between them. Thus, the intercalated Fe dopants are a key factor for the magnitude of MM and MEC of Fe-doped bilayer MoS_2.

4. DISCUSSION

The above results indicate that FM coupling is energetically favorable in Fe-doped monolayer MoS_2 and that AFM coupling is preferred in the bilayer one for most allowed chemical potentials, in particular for the S-rich condition. This implies that the layer number may have an important effect on magnetic properties of Fe-doped MoS_2 nanosheets. To understand the role of layer number in the MEC of Fe-doped MoS_2 sheets, trilayer MoS_2 with Fe dopants have been investigated. The doping configurations and formation energies of Fe-doped three-layer MoS_2 have been shown in Figures S3 and S4 in the Supporting Information. For the trilayer MoS_2 with two Fe dopants (see Figure S5 in the Supporting Information), its doping stability is similar to that of the bilayer MoS_2 mentioned above. Namely, Fe_SFe_i, Fe_iFe_i, and $Fe_{Mo}Fe_i$ are the most stable doping structure in sequence as the chemical potential changes from the Mo-rich to the S-rich conditions. For the trilayer MoS_2 with four Fe dopant atoms (Figure S6 in the Supporting Information), the $(Fe_iFe_i)_2$ is energetically favorable under the Mo-rich condition and the $(Fe_{Mo}Fe_i)_2$ is stable in the S-rich regime. On the basis of above results, $(Fe_{Mo}Fe_i)_n$ (n = 1, 2) should be thermodynamically stable in the multilayer MoS_2 on the basis of the fact that the synthesis of MoS_2 nanosheets was generally maintained under the S-rich condition. The energy comparison indicated that $Fe_{Mo}Fe_i$ and $(Fe_{Mo}Fe_i)_2$ structures of trilayer MoS_2 with the AFM coupling are 64 and 181 meV lower than that with the FM coupling, respectively. Moreover, we find that highly spin-polarized Fe atoms in both $Fe_{Mo}Fe_i$ and $(Fe_{Mo}Fe_i)_2$ structures exhibit antiparallel SP direction each other, as shown in Figure 7. Therefore, the AFM coupling should also be favorable in trilayer Fe-doped MoS_2 nanosheets.

Because of the introduction of two or more Fe dopant atoms into MoS_2 nanosheets, the magnetic coupling will depend on the successive spin correlations. The magnetic coupling based on the successive spin polarizations has been discussed widely in previous studies.[25,53,55,56] For instance, an enhancement of the magnetism in MoS_2 can be realized by the codoping because of the formation of successive local spin correlations that act to oppose the superexchange coupling.[25] Introducing a magnetic bipartite chain into ZnO and GaN lattices was found to enhance the stability of FM state and the FM coupling among magnetic dopants was viewed as a generalization of the classical interatomic double- exchange and superexchange

DOI: 10.1021/am508843z
ACS Appl. Mater. Interfaces 2015, 7, 7534−7541

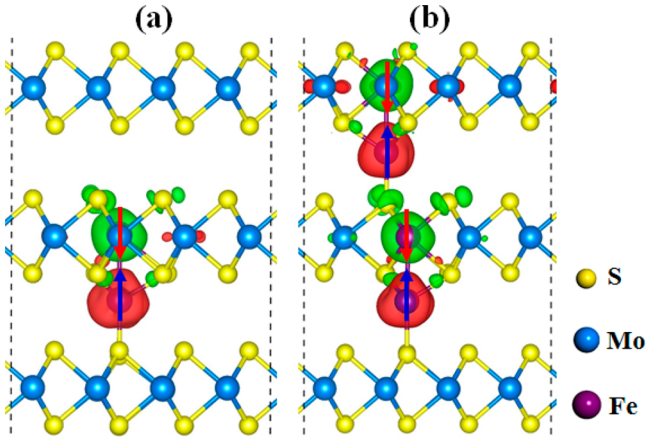

Figure 7. Spin-density ($\rho\uparrow - \rho\downarrow$) isosurface distributions of Fe-doped trilayer MoS_2 nanosheets: (a) $Fe_{Mo}Fe_i$ and (b) $Fe_{Mo}Fe_i$-$Fe_{Mo}Fe_i$. The red and green isosurfaces represent positive and negative spin density, respectively. The blue and red arrows denote the opposite direction of spin polarization.

interactions.[56] These results were obtained on the basis of the doping models in which all TM dopants occupy at the substitutional sites. However, the stable Fe-doped MoS_2 structures in the present study contain both intercalated and substitutional Fe dopants. The formation of direct and mediated bonding interactions between two types of Fe dopants follows the superexchange mechanism.

On the basis of above analysis, the MEC of Fe dopant atoms in MoS_2 nanosheets actually depends on the competition between double-exchange interaction and superexchange interaction.[54] For the Fe doping in monolayer MoS_2, the substitutional Fe dopants at Mo sites are coupled ferromagnetically via the double-exchange mechanism. Moreover, the Fe dopants with the FM coupling are mediated by the hybridization between Fe-3d states and S-2p states, which results in the AFM coupling between the Fe dopants and the nearest neighboring S atoms (see Figure 8a). A similar mechanism was demonstrated in a lot of semiconductors and other 2D systems.[26,53,57−59] For Fe-doped bilayer and multilayer MoS_2 nanosheets, the formation of $Fe_{Mo}Fe_i$ structures leads to a direct and mediated bonding interaction between dopants. Therefore, the d-electrons interaction among Fe dopants follows the superexchange mechanism, resulting in the antiparallel SP

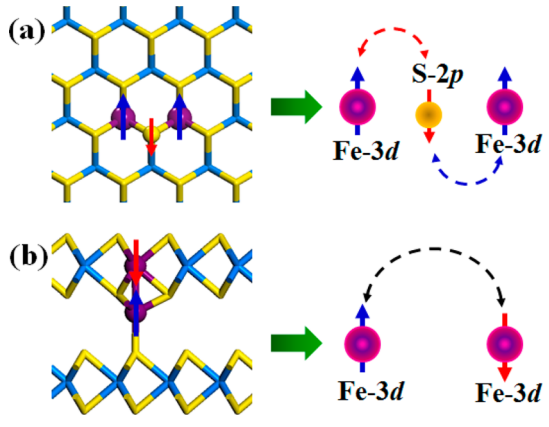

Figure 8. Schematic models of (a) double-exchange mechanism and (b) superexchange mechanism in Fe-doped MoS_2 nanosheets.

among neighboring Fe dopants (Figure 8b). Hence, the AFM coupling is favored in Fe-doped MoS_2 sheets when the layer number is beyond two layers.

5. CONCLUSIONS

In summary, we performed a detailed theoretical investigation on the dopant stability, electronic and magnetic properties of Fe-doped monolayer, bilayer, and trilayer MoS_2 nanosheets. The calculated formation energies indicate that the geometry and the stability of Fe dopant atoms in MoS_2 strongly depend on the chemical potential and the layer number. Under an S-rich environment that is generally adopted condition to synthesize MoS_2 nanosheets, Fe_{Mo} dopants in monolayer MoS_2 are stable and $Fe_{Mo}Fe_i$ complexes are energetically more favorable in bilayer and multilayer MoS_2 sheets. The introduction of Fe dopants into MoS_2 leads to the FM coupling in the monolayer sheet and the AFM coupling in bilayer and multilayer ones, suggesting the layer dependence of MEC in the Fe-doped MoS_2. The layer dependence of MEC originates from the competition mechanism between the double-exchange and superexchange interactions. More specifically, the magnetic coupling of Fe dopants in the monolayer MoS_2 via the double-exchange mechanism can be mediated by S-2p states, favoring the FM coupling. In contrast, the superexchange mechanism is preferred in bilayer and multilayer MoS_2 sheets (layer number $\geq$2), leading to the AFM coupling. Therefore, the realization of ferromagnetism in Fe-doped MoS_2 requires the precise control of the layer number during the synthesis.

■ ASSOCIATED CONTENT

Supporting Information

The detail for the determination of U_{eff} parameter, spin-density distribution of isolated Fe dopant in monolayer MoS_2, spin band structures of isolated Fe dopants in monolayer MoS_2, doping configurations and formation energies of two Fe dopants in trilayer MoS_2, and doping configurations and formation energies of four Fe dopants in trilayer MoS_2. This material is available free of charge via the Internet at http://pubs.acs.org.

■ AUTHOR INFORMATION

Corresponding Author

*E-mail: shu123hb@gmail.com. Phone: +86-0571-86875622.

Notes

The authors declare no competing financial interest.

■ ACKNOWLEDGMENTS

This work was supported in part by the National Natural Science Foundation of China (Grants 11404309, 11347109, 11347106, 51402275), Zhejiang Provincial Natural Science Foundation of China (LQ13A040001). Computational resources from the Shanghai Supercomputer Center are acknowledged.

■ REFERENCES

(1) Novoselov, K. S.; Geim, A. K.; Morozov, S. V.; Jiang, D.; Zhang, Y.; Dubonos, S. V.; Grigorieva, I. V.; Firsov, A. A. Electric Field Effect in Atomically Thin Carbon Films. *Science* **2004**, *306*, 666−669.

(2) Levendorf, M. P.; Kim, C.-J.; Brown, L.; Huang, P. Y.; Havener, R. W.; Muller, D. A.; Park, J. Graphene and Boron Nitride Lateral Heterostructures for Atomically Thin Circuitry. *Nature* **2012**, *488*, 627−632.

DOI: 10.1021/am508843z
ACS Appl. Mater. Interfaces 2015, 7, 7534−7541

(3) Vogt, P.; Padova, P. D.; Quaresima, C.; Avila, J.; Frantzeskakis, E.; Asensio, M. C.; Resta, A.; Ealet, B.; Lay, G. L. Silicene: Compelling Experimental Evidence for Graphenelike Two-Dimensional Silicon. *Phys. Rev. Lett.* **2012**, *108*, 155501.
(4) Wang, Q. H.; Kalantar-Zadeh, K.; Kis, A.; Coleman, J. N.; Strano, M. S. Electronics and Optoelectronics of Two-Dimensional Transition Metal Dichalcogenides. *Nat. Nanotechnol.* **2012**, *7*, 699−712.
(5) Chhowalla, M.; Shin, H. S.; Eda, G.; Li, L.-J.; Loh, K. P.; Zhang, H. The Chemistry of Two-Dimensional Layered Transition Metal Dichalcogenide Nanosheets. *Nat. Chem.* **2013**, *5*, 263−275.
(6) Jariwala, D.; Sangwan, V. K.; Lauhon, L. J.; Marks, T. J.; Hersam, M. C. Emerging Device Applications for Semiconducting Two-Dimensional Transition Metal Dichalcogenides. *ACS Nano* **2014**, *8*, 1102−1120.
(7) Mak, K. F.; Lee, C.; Hone, J.; Shan, J.; Heinz, T. F. Atomically Thin MoS_2: A New Direct-Gap Semiconductor. *Phys. Rev. Lett.* **2010**, *105*, 136805.
(8) Wang, K.; Wang, J.; Fan, J.; Lotya, M.; O'Neill, A.; Fox, D.; Feng, Y.; Zhang, X.; Jiang, B.; Zhao, Q.; Zhang, H.; Coleman, J. N.; Zhang, L.; Blau, W. J. Ultrafast Saturable Absorption of Two-Dimensional MoS_2 Nanosheets. *ACS Nano* **2013**, *7*, 9260−9267.
(9) Lukowski, M. A.; Daniel, A. S.; Meng, F.; Forticaux, A.; Li, L.; Jin, S. Enhanced Hydrogen Evolution Catalysis from Chemically Exfoliated Metallic MoS_2 Nanosheets. *J. Am. Chem. Soc.* **2013**, *135*, 10274−10277.
(10) Zeng, H.; Dai, J.; Yao, W.; Xiao, D.; Cui, X. Valley Polarization in MoS2Monolayers by Optical Pumping. *Nat. Nanotechnol.* **2012**, *7*, 490−493.
(11) Min, S.-W.; Lee, H. S.; Choi, H. J.; Park, M. K.; Nam, T.; Kim, H.; Ryu, S.; Im, S. Nanosheet Thickness-Modulated MoS_2 Dielectric Property Evidenced by Field-Effect Transistor Performance. *Nanoscale* **2013**, *5*, 548−551.
(12) Lee, H. S.; Min, S.-W.; Chang, Y.-G.; Park, M. K.; Nam, T.; Kim, H.; Kim, J. H.; Ryu, S.; Im, S. MoS_2 Nanosheet Phototransistors with Thickness-Modulated Optical Energy Gap. *Nano Lett.* **2012**, *12*, 3695−3700.
(13) Wu, S.; Zeng, Z.; He, Q.; Wang, Z.; Wang, S. J.; Du, Y.; Yin, Z.; Sun, X.; Chen, W.; Zhang, H. Electrochemically Reduced Single-Layer MoS_2 Nanosheets: Characterization, Properties, and Sensing Applications. *Small* **2012**, *8*, 2264−2270.
(14) Stephenson, T.; Li, Z.; Olsen, B.; Mitlin, D. Lithium Ion Battery Applications of Molybdenum Disulfide (MoS_2) Nanocomposites. *Energy Environ. Sci.* **2014**, *7*, 209−231.
(15) Cheng, Y. C.; Nie, A.; Zhang, Q.; Gan, L.-Y.; Shahbazian-Yassar, R.; Schwingenschlogl, U. Origin of the Phase Transition in Lithiated Molybdenum Disulfide. *ACS Nano* **2014**, *8*, 11447−11453.
(16) Benck, J. D.; Hellstern, T. R.; Kibsgaard, J.; Chakthranont, P.; Jaramillo, T. F. Catalyzing the Hydrogen Evolution Reaction (HER) with Molybdenum Sulfide Nanomaterials. *ACS Catal.* **2014**, *4*, 3957−3971.
(17) Mathew, S.; Gopinadhan, K.; Chan, T. K.; Yu, X. J.; Zhan, D.; Cao, L.; Rusydi, A.; Breese, M. B. H.; Dhar, S.; Shen, Z. X.; Venkatesan, T.; Thong, J. T. L. Magnetism in MoS_2 induced by Proton Irradiation. *Appl. Phys. Lett.* **2012**, *101*, 102103.
(18) Zhang, Z.; Zou, X.; Crespi, V. H.; Yakobson, B. I. Intrinsic Magnetism of Grain Boundaries in Two-Dimensional Metal Dichalcogenides. *ACS Nano* **2013**, *7*, 10475−10481.
(19) Shi, H. L.; Pan, H.; Zhang, Y.-W.; Yakobson, B. I. Strong Ferromagnetism in Hydrogenated MoS_2 tuned by stain. *Phys. Rev. B* **2013**, *88*, 205305.
(20) Li, Y.; Zhou, Z.; Zhang, S.; Chen, Z. MoS_2 Nanoribbons: High Stability and Unusual Electronic and Magnetic Properties. *J. Am. Chem. Soc.* **2008**, *130*, 16739−16744.
(21) Gao, D.; Si, M.; Li, J.; Zhang, J.; Zhang, Z.; Yang, Z.; Xue, D. Ferromagnetism in Freestanding MoS_2 Nanosheets. *Nanoscale Res. Lett.* **2013**, *8*, 129.
(22) Chen, Q.; Ouyang, X.; Yuan, S.; Li, R.; Wang, J. Uniformly Wetting Deposition of Co atoms on MoS2 monolayer: A Promising Two-Dimensional Robust Half-Metallic Ferromagnet. *ACS Appl. Mater. Interfaces* **2014**, *6*, 16835−16840.
(23) Wang, S. Y.; Ko, T. S.; Huang, C. C.; Lin, D. Y.; Huang, Y. S. Optical and Electrical Properties of MoS_2 and Fe-doped MoS_2. *Jpn. J. Appl. Phys.* **2014**, *53*, 04EH07.
(24) Cheng, Y. C.; Zhu, Z. Y.; Mi, W. B.; Guo, Z. B.; Schwingenschlögl, U. Prediction of Two-Dimensional Diluted Magnetic Semiconductors: Doped Monolayer MoS_2 systems. *Phys. Rev. B* **2013**, *87*, 100401(R).
(25) Andriotis, A. N.; Menon, M. Tunable Magnetic Properties of Transition Metal Doped MoS_2. *Phys. Rev. B* **2014**, *90*, 125304.
(26) Ramasubramaniam, A.; Naveh, D. Mn-Doped Monolayer MoS_2: An Atomically Thin Dilute Magnetic Semiconductor. *Phys. Rev. B* **2013**, *87*, 195201.
(27) Yun, W.; Lee, J. D. Unexpected Strong Magnetism of Cu Doped Single-Layer MoS_2 and Its Origin. *Phys. Chem. Chem. Phys.* **2014**, *16*, 8990−8996.
(28) Komsa, H.-P.; Berseneva, N.; Krasheninnikov, A. V.; Nieminen, R. M. Charged Point Defects in the Flatland: Accurate Formation Energy Calculations in Two-Dimensional Materials. *Phys. Rev. X* **2014**, *4*, 031044.
(29) Lin, X. Q.; Ni, J. Charge and Magnetic States of Mn-, Fe-, and Co-doped Monolayer MoS_2. *J. Appl. Phys.* **2014**, *116*, 044311.
(30) Kan, M.; Adhikari, S.; Sun, Q. Ferromagnetism in MnX_2 (X = S, Se) Monolayer. *Phys. Chem. Chem. Phys.* **2014**, *16*, 4990−4994.
(31) Dolui, K.; Rungger, I.; Pemmaraju, C. D.; Sanvito, S. Possible Doping Strategies for MoS_2 Monolayers: An ab initio Study. *Phys. Rev. B* **2013**, *88*, 075420.
(32) Feng, N.; Mi, W.; Cheng, Y.; Guo, Z.; Schwingenschlögl, U.; Bai, H. First Principles Prediction of the Magnetic Properties of Fe-X_6 (X = S, C, N, O, F) Doped Monolayer MoS_2. *Sci. Rep.* **2014**, *4*, 3978.
(33) Huang, Z.; Peng, X.; Yang, H.; He, C.; Xue, L.; Hao, G.; Zhang, C.; Liu, W.; Qi, X.; Zhong, J. The structural, Electronic and Magnetic Properties of Bilayered MoS_2 with Transition-Metals Doped in the Interlayer. *RSC Adv.* **2013**, *3*, 12939.
(34) Huang, Z.; Hao, G.; He, C.; Yang, H.; Xue, L.; Qi, X.; Peng, X.; Zhong, J. X. Density Functional Theory Study of Fe Adatoms Adsorbed Monolayer and Bilayer MoS_2 Sheets. *J. Appl. Phys.* **2013**, *114*, 083706.
(35) Zhou, W.; Zou, X.; Najmaei, S.; Liu, Z.; Shi, Y.; Kong, J.; Lou, J.; Ajayan, P. M.; Yakobson, B. I.; Idrobo, J.-C. Intrisic Structural Defects in Monolayer Disufide. *Nano Lett.* **2013**, *13*, 2615−2622.
(36) Blöchl, P. E. Projector Augmented-Wave Method. *Phys. Rev. B* **1994**, *50*, 17953−17979.
(37) Kresse, G.; Furthmüller, J. Efficient Iterative Schemes for *Ab Initio* Total-Energy Calculations Using a Plane-Wave Basis Set. *Phys. Rev. B* **1996**, *54*, 11169−11186.
(38) Payne, M. C.; Teter, M. P.; Allan, D. C.; Arias, T. A.; Joannopoulos, J. D. Iterative Minimization Techniques for *Ab Initio* Total-Energy Calculations: Molecular Dynamics and Conjugate Gradients. *Rev. Mod. Phys.* **1992**, *64*, 1045−1097.
(39) Cococcioni, M.; de Gironcoli, S. Linear Response Approach to the Calculation of the Effective Interaction Parameters in the LDA+U method. *Phys. Rev. B* **2005**, *71*, 035105.
(40) Ederer, C.; Spaldin, N. A. Origin of Ferroelectricity in the Multiferroic Barium Fluorides $BaMF_4$: A First Principles Study. *Phys. Rev. B* **2006**, *74*, 024102.
(41) Rollmann, G.; Rohrbach, A.; Entel, P.; Hafner, J. First-Principles Calculation of the Structure and Magnetic Phases of Hematite. *Phys. Rev. B* **2004**, *69*, 165107.
(42) Jeng, H.-T.; Guo, G. Y.; Huang, D. J. Charge-Orbital Ordering and Verwey Transition in Magnetite. *Phys. Rev. Lett.* **2004**, *93*, 156403.
(43) Kresse, G.; Joubert, D. From Ultrasoft Pseudopentials to the Projector Augmented-Wave Methods. *Phys. Rev. B* **1999**, *59*, 1758−1775.
(44) Tang, W.; Sanville, E.; Henkelman, G. A Grid-Based Bader Analysis Algorithm without Lattice Bias. *J. Phys.: Condens. Matter.* **2009**, *21*, 084204.

DOI: 10.1021/am508843z
ACS Appl. Mater. Interfaces 2015, 7, 7534−7541

(45) Bader, R. F. W. A Quantum Theory of Molecular Structure and Its Applications. *Chem. Rev.* **1991**, *91*, 893−928.
(46) Suh, J.; Park, T.-E.; Lin, D.-Y.; Fu, D.; Park, J.; Jung, H. J.; Chen, Y.; Ko, C.; Jang, C.; Sun, Y.; Sinclair, R.; Chang, J.; Tongay, S.; Wu, J. Doping Against the Native Propensity of MoS_2: Degenerate Hole Doping by Cation Substitution. *Nano Lett.* **2014**, *14*, 6976−6982.
(47) Van der Zande, A. M.; Huang, P. Y.; Chenet, D. A.; Berkelbach, T. C.; You, Y. M.; Lee, G.-H.; Heinz, T. F.; Reichman, D. R.; Muller, D. A.; Hone, J. C. Grains and Grain Boundaries in Highly Crystalline Monolayer Molybdenum Disulphide. *Nat. Mater.* **2013**, *12*, 554−561.
(48) Najmaei, S.; Liu, Z.; Zhou, W.; Zou, X.; Shi, G.; Lei, S.; Yakobson, B. I.; Idrobo, J.-C.; Ajayan, P. M.; Lou, J. Vapour Phase Growth and Grain Boundary Structure of Molybdenum Disulphide Atomic layers. *Nat. Mater.* **2013**, *12*, 754−759.
(49) Cheng, Y.; Nie, A.; Zhang, Q.; Gan, L. Y.; Shahbazian-Yassar, R.; Schwingenlogl, U. Origin of the Phase Transition in Lithiated Molybdenum Disulphide. *ACS Nano* **2014**, *8*, 11447−11453.
(50) Wang, X. F.; Shen, X.; Wang, Z. X.; Yu, R.; Chen, L. Q. Atomic-Scale Clarification of Structural Transition of MoS_2 upon Sodium Intercalation. *ACS Nano* **2014**, *8*, 11394−11400.
(51) Kudrnovský, J.; Turek, I.; Drchal, V.; Máca, F.; Weinberger, P.; Bruno, P. Exchange Interactions in III-V and Group-IV Diluted Magnetic Semiconductors. *Phys. Rev. B* **2004**, *69*, 115208.
(52) Kan, M.; Zhou, J.; Sun, Q.; Kawazoe, Y.; Jena, P. The Intrinsic Ferromagnetism in a MnO_2 Monolayer. *J. Phys. Chem. Lett.* **2013**, *4*, 3382−3386.
(53) Mishra, R.; Zhou, W.; Pennycook, S. J.; Pantelides, S. T.; Idrobo, J.-C. Long-Range Ferromagnetic Ordering in Manganese-Doped Two-Dimensional Dichalcogenides. *Phys. Rev. B* **2013**, *88*, 144409.
(54) Sato, K.; Bergqvist, L.; Kudrnovsky, J.; Dederichs, P. H.; Eriksson, O.; Turek, I.; Sanyal, B.; Bouzerar, G.; Katayama-Yoshida, H.; Dinh, V. A.; Fukushima, T.; Kizaki, H.; Zeller, R. First-Principles Theory of Dilute Magnetic Semiconductors. *Rev. Mod. Phys.* **2010**, *82*, 1633−690.
(55) Andriotis, A. N.; Lisen1kov, S.; Menon, M. Ferromagnetic Interactions in Hosted Bipartite Materials-Generalized-Double-Exchange and Generalized-Superexchange Interactions. *J. Phys.: Condens. Matter* **2011**, *23*, 086004.
(56) Andriotis, A. N.; Menon, M. Defect-Induced Magnetism: Codoping and A Prescription for Enhanced Magnetism. *Phys. Rev. B* **2013**, *87*, 155309.
(57) Ma, Y.; Dai, Y.; Guo, M.; Niu, C.; Zhu, Y.; Huang, B. Evidence of the Existence of Magnetism in Pristine VX_2 Monolayers (X = S, Se) and Their Strain-Induced Tunable Magnetic Properties. *ACS Nano* **2012**, *2*, 1695−1701.
(58) He, J. J.; Zhou, P.; Jiao, N.; Ma, S. Y.; Zhang, K. W.; Wang, R. Z.; Sun, L. Z. Magnetic Exchange Coupling and Anisotropy of 3d Transition Metal Nanowires and Graphyne. *Sci. Rep.* **2014**, *4*, 4014.
(59) Khazaei, M.; Arai, M.; Sasaki, T.; Chung, C.-Y.; Venkataramanan, N. S.; Estili, M.; Sakka, Y.; Kawazoe, Y. Novel Electronic and Magnetic Properties of Two-Dimensional Transition Metal Carbides and Nitrides. *Adv. Funct. Mater.* **2013**, *23*, 2185−2192.

DOI: 10.1021/am508843z
ACS Appl. Mater. Interfaces 2015, 7, 7534−7541